THE JOURNAL OF PHYSICAL CHEMISTRY C

Article

pubs.acs.org/JPCC

Structure Determination of Superatom Metallic Clusters Using Rapid Scanning Electron Diffraction

Alina Bruma,[†] Ulises Santiago,[†] Diego Alducin,[†] German Plascencia Villa,[†] Robert L. Whetten,[†] Arturo Ponce,[†] Marcelo Mariscal,[‡] and Miguel José-Yacamán*[,†]

[†]Department of Physics and Astronomy, The University of Texas at San Antonio, One UTSA Circle, San Antonio, 78249, United States

[‡]School of Chemical Sciences, National University of Cordoba, Avenue Haya de la Torre Cordoba, Cordoba, 5000, Argentina

Supporting Information

ABSTRACT: Experimental analysis of electron diffraction patterns for ligand-stabilized gold clusters in transmission electron microscopy is a cumbersome procedure, due to electron beam−induced irradiation damage. We propose herein a method for instantaneous data collection using scanning nanobeam electron diffraction and the subsequent determination of the crystal metallic clusters. The procedure has been tested on a known structure, namely $Au_{102}(p\text{-MBA})_{44}$ nanoclusters and has been compared with their structure theoretically determined by ones previously obtained from X-ray diffraction analysis. The method can be unambiguously applied for the case of any nanoscale system susceptible to electron beam damage and it is capable to register the rotation effect on the metallic clusters caused due to the electron beam interaction during the raster scanning on the sample.

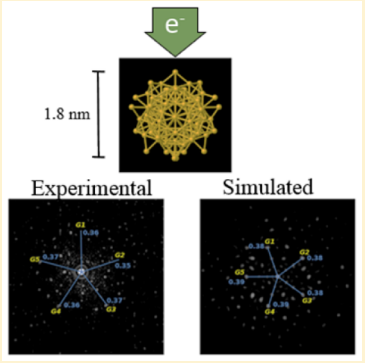

1. INTRODUCTION

The first report on successful crystallization of ligand-protected *p*-mercaptobenzoic acid $(p\text{-MBA})_{44}$ Au_{102} nanoclusters published by Jadzinsky et al.[1] allowed the structural characterization of thiolate protected clusters, opening the way to a completely new array of applications. The $Au_{102}(p\text{-MBA})_{44}$ nanoclusters recently became the subject of study in biolabeling analyses for site-specific covalent conjugation to viral surfaces,[2] photodynamics[3] and nanocatalysis.[4] A precise knowledge of the nanoclusters' atomic structure is crucial for correlations with their catalytic, electronic, and optical properties. X-ray crystallography is one of the most reliable approaches for a thorough determination of nanoclusters structures.[5] However, high-quality single-crystal samples must be synthesized in order to achieve characterization using X-ray diffraction. Until now, solving the structure using X-ray analysis has been achieved for just several Au nanoclusters: $Au_{25}[SR]_{18}$,[6,7] $Au_{38}[SR]_{24}$,[8] and $Au_{102}[SR]_{44}$.[1] Electron diffraction analysis in transmission electron microscopy (TEM) is still an extremely problematic issue due to electron beam irradiation damage. There are two main damage mechanisms that can appear in the ligand-protected clusters during the acquisition for images and nanobeam diffraction patterns (NBD) in the TEM: (i) the knock-on effect, arising from the momentum transfer between the electron beam and the nanoclusters,[9] and (ii) the ionization damage (radiolysis).[10] Mass loss from clusters structure following electron beam irradiation can preclude structural characterization. Certain conditions must be satisfied in order to declare that the observed electron diffraction patterns are significant for the case of nanoclusters susceptible to beam damage: they must show stability for several milliseconds; i.e., they are the *representative* patterns registered under rapid acquisition and ultralow dose irradiation, in order to preserve not only the initial number of atoms in the nanoclusters structures, but to ensure that the thiolate-ligands are not damaged.

For small nanoclusters, in order to interpret the experimental electron diffraction patterns, they must be calculated and quantitatively compared with simulated ones obtained from structural models, since at the observed sizes (<2 nm), the shape effects are extremely strong.[9,11] Although significant efforts have been employed to minimize as much as possible the damaging effect of the electron beam on the nanoclusters during diffraction patterns acquisition,[12,13] it has been acknowledged that irreversible structural changes are hard to avoid in small, ligand protected nanoclusters, and permanent damage of the sulfur−gold bonds in the nanoclusters capping layer can occur. In this paper we report a technique for acquiring NBD patterns at millisecond rate, involving an ultralow dose, which can be used for all nanoscale systems susceptible to electron beam damage. The acquired patterns accomplish the conditions mentioned above and unambiguous structural characterization of nanoclusters is successfully achieved. We have tested our method on $Au_{102}(p\text{-MBA})_{44}$ nanoclusters, since the structure is

Received: September 29, 2015
Revised: December 18, 2015

DOI: 10.1021/acs.jpcc.5b09524
J. Phys. Chem. C XXXX, XXX, XXX−XXX

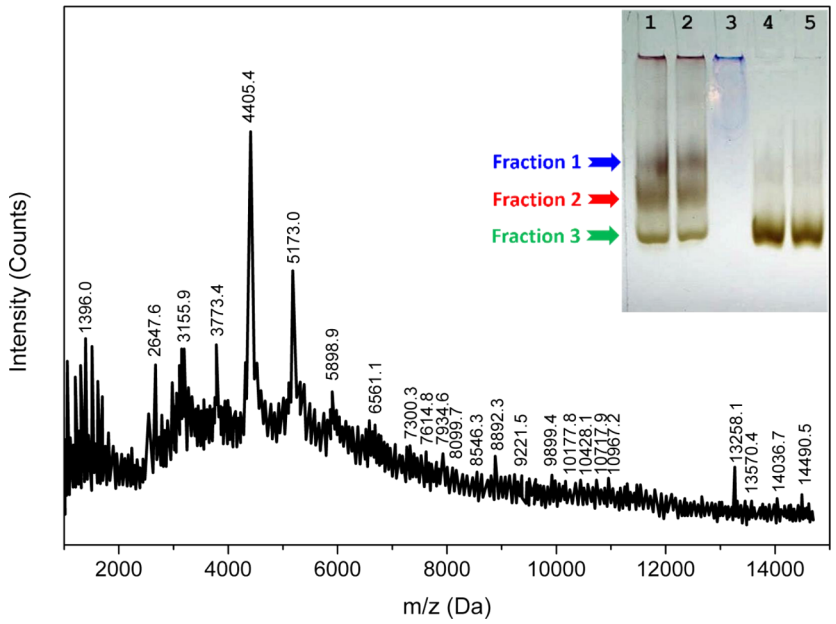

Figure 1. ESI–MS emphasizing the $Au_{102}(p\text{-MBA})_{44}$ species. The inset shows a native PAGE electrophoresis: (1, 2) Au(*p*-MBA) nanoclusters with three particle sizes; (3) loading buffer; (4, 5) Au_{102} enriched fraction. Pellets 4 and 5 (single fractions) correspond to the samples used for TEM/STEM characterization.

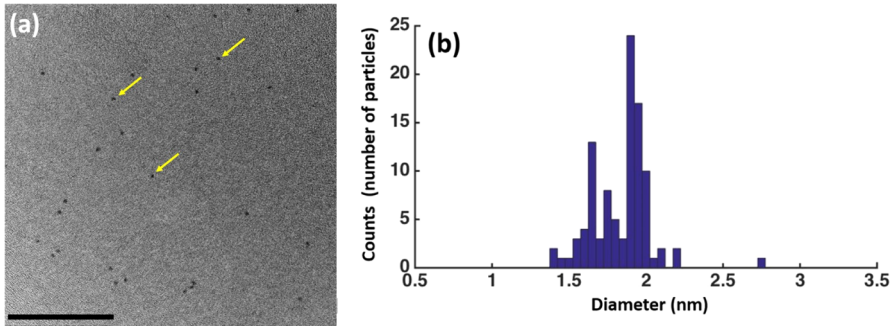

Figure 2. (a) Example of an area on the sample before the acquisition of nanobeam diffraction patterns using the ASTAR system in a conventional JEOL 2010F TEM microscope. $Au_{102}(p\text{-MBA})_{44}$ nanoclusters are visible, marked by arrow pointers (scale bar = 40 nm). (b) Histogram of the size distribution of the $Au_{102}(p\text{-MBA})_{44}$ nanoclusters.

well-known, model is available in Figure S1 of the Supporting Information.[14,15] Here, the electron probe is scanned on a pre-established area, without the need of an *in-built* Scanning transmission electron microscope (STEM),[16] a method developed and employed with preponderance in precession diffraction.[17] The NBD patterns are recorded as a video with a high sensitive CMOS camera, as a set-series, from all the clusters in the field of view. The video is recorded by means of a line-by-line sweep and subsequently is divided in individual images and these are processed to be compared with their counterparts patterns simulated. Using this methodology, we have been able to acquire NBD patterns at milliseconds rate, much before any irreversible change in the cluster structure may arise following electron beam irradiation. Since the $Au_{102}(p\text{-MBA})_{44}$ nanoclusters are in random zone axes, this method offers the possibility of obtaining structural information for hundreds of such nanoclusters in a single scan and to build a structural "atlas" in reciprocal space.

2. EXPERIMENTAL SECTION

2.1. Sample Preparation and Mass Spectrometry. We have synthesized the $Au_{102}(p\text{-MBA})_{44}$ nanoclusters by the two-phase transfer method.[1] First, 4-mercaptobenzoic acid (*p*-MBA) was dissolved in 0.3 M NaOH aqueous solution by stirring for at least 6 h. Au nanoclusters were prepared in 25 mL batches in 50% methanol v/v, by adding $HAuCl_4$ to a final concentration of 3 mM and *p*-MBA at 9 mM final concentration. The solution was vigorously stirred overnight until mixture was colorless. Subsequently, ice-cold $NaBH_4$ was added to a final concentration of 4.5 mM with vigorous stirring for 2 h. Finally, the entire reaction was placed in a 50 mL conical tube with 1 volume of cold methanol and placed at 4 °C to allow precipitation. Au NC were concentrated by centrifugation (1000 rpm for 10 min), the pellet resuspended in cold methanol and centrifuged again to remove byproducts. Finally, Au nanoclusters were air-dried and dissolved in a small volume of dd H_2O. The quality of Au nanoclusters was assessed by nondenaturing polyacrylamide gel electrophoresis (PAGE), as shown in the inset Figure 1. Samples were passed through a 10% native gel (19:1) in 1X TBE (Tris–Borate–EDTA) buffer

DOI: 10.1021/acs.jpcc.5b09524
J. Phys. Chem. C XXXX, XXX, XXX–XXX

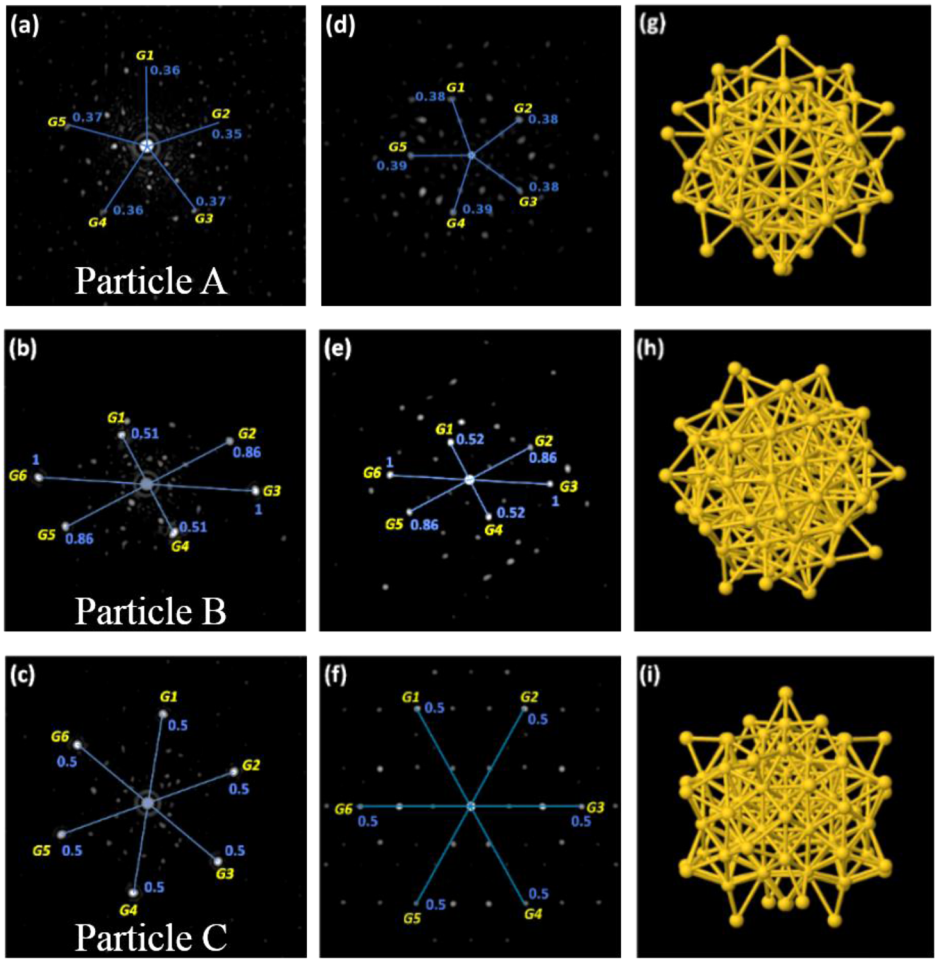

Figure 3. (a–c) Three experimentally acquired nanobeam diffraction patterns for three particles are emphasised, labeled A, B and C; (d–f) the simulated counterparts of nanoclusters from parts a–c; (g–i) corresponding structural models used for simulations in parts d–f.

at 100–110 V for around 90 min. The inset in Figure 1 shows the clear separation of sizes, with fractions 1, 2, and 3 corresponding to pellets 1 and 2 being assigned to the sizes Au_{228}, Au_{144} and Au_{102}, respectively, and pellets 4 and 5 containing the purified, $Au_{102}(p\text{-MBA})_{44}$ nanoclusters used in this experiment. The corresponding electrospray ionization mass spectrum (ESI–MS) is shown in Figure 1 and discussed in detail in section S1 of Supporting Information.

2.2. Electron Microscopy Characterization. The samples were characterized by TEM and scanning NBD, experimental set up is shown in the Figure S2 of the Supporting Information. The TEM sample grid was prepared by placing 3–4 drops of dilute solution on a carbon film-coated Ni mesh (3 mm diameter, 400 mesh) covered with holes and dried in air at room temperature. The acquisition of ultralow dose diffraction patterns was made using a JEOL 2010 F operating at 200 kV acceleration voltage, with a beam current of 1.9 pA/cm^2 and a probe size of 3 nm, to which a NAMOMEGAS ASTAR system[16,18] has been coupled, allowing the fast scan of the electron beam on a pre-established area, followed by the collection of the NBD patterns (see Figure 2). The JEOL 2010 F microscope has been equipped with an ultrafast TVIPS 16-mega pixel F416 CMOS camera with a dynamic range (max./noise) of 10000:1.[19,20] See details in section S2 of Supporting Information.

3. RESULTS AND DISCUSSION

Figure 2 shows a low-magnification TEM image of an area of the sample showing the $Au_{102}(p\text{-MBA})_{44}$ nanoclusters supported on *a-C* substrate acquired before our series of NBD diffraction patterns are recorded. The mean size of the $Au_{102}(p\text{-MBA})_{44}$ nanoclusters is 1.84 ± 0.18 nm, as emphasized by the size distribution in Figure 2b where 100 nanoclusters have been taken into consideration. It is important to mention that, during the serial acquisition of the patterns, TEM images of the scanned area are not recorded simultaneously. However, a combined approach of ultrafast nanobeam diffraction and electron diffraction simulation based on a structural model - are used to extract structural information about the $Au_{102}(p\text{-MBA})_{44}$ nanoclusters. Our diffraction patterns were acquired using a CMOS camera fitted into a JEOL 2010F that was chosen over a conventional CCD camera. The choice was based on the resolution of two camera sensors. The CMOS camera has a 16 bit resolution when compared to the 12 bit resolution of the CCD camera, offering a higher dynamic range and quality of images.[16,17] Also, CMOS sensors help eliminate the problem of streaking suffered by the CCD sensors. CCD is a capacitive array with a photoactive region, i.e., when an image is projected onto the surface of a CCD it results in charge accumulation in the capacitive wells that is proportional to the intensity of light falling on it. On the basis of the design of the CCD, there is a maximum amount of charge that can be

DOI: 10.1021/acs.jpcc.5b09524
J. Phys. Chem. C XXXX, XXX, XXX–XXX

accumulated in each pixel termed as the saturation charge level. When this level is exceeded, charge begins to leak into the neighboring wells, resulting in the phenomenon of blooming. The direction of electron or charge flow depends on the structure of the CCD and results in vertical streaking. In Figure S3a of the Supporting Information we are showing a NBD pattern acquired using the CCD camera fitted in a JEOL ARM 200F, using the same exposure conditions as the ones we use for our ultralow dose NBD patterns acquisition using the JEOL 2010F fitted with the CMOS camera (Figure S3b of the Supporting Information). Although the probe size is sharper compared to our JEOL 2010F, the phenomenon of vertical streaking is visible and moreover.

Figures 3a-c emphasize three experimentally acquired nanobeam diffraction patterns for three particles, labeled A, B, and C, their simulated counterparts in Figure 3d–f, together with the corresponding structural models used for simulations in Figure 3g–i. Moreover, in Table 1, we are emphasizing the

Table 1. Measurements Comparing the Experimental NBD Patterns with the Simulated Electron Diffraction Patterns in Figure 3

		angle (deg)	
particle	spot	experimental pattern	simulated pattern
A	G_1	72.7	72.4
	G_2	73.9	72.6
	G_3	71.5	71.4
	G_4	71.3	71.7
	G_5	70.9	72.1
B	G_1	90	89
	G_2	31.4	31
	G_3	58.5	59.2
	G_4	89.9	89.9
	G_5	31.2	30.8
	G_6	58.5	59.2
C	G_1	60	58.1
	G_2	60	61
	G_3	60	61
	G_4	60	58.1
	G_5	60	61
	G_6	60	60

calculated values of angles between the *g*-vectors for each case. The simulated diffraction patterns have been generated by using the *xyz* cluster coordinates provided in ref 14. Those coordinates are very reliable since were obtained by X-ray diffraction of a monocrystal of clusters.The electron diffraction simulations were performed using the module "Nanodiffraction" in the Java Electron Microscopy Software (JEMS).[21,22] Experimentally equivalent parameters were used as inputs to the JEMS software for the calculations. Our method allows collection of diffraction patterns at the milisec rate. We start to record patterns until a drastic change is observed. It is well established on the literature that surface free nanoparticles tend to have a fluctuating structure.[23−26] In this way, when we start the recording of diffraction patterns we apply the criteria that if at least 10 sequential patters are recorded showing the same structure, which corresponds to the pristine cluster structure. It was clearly observed that when radiation damage (radiolysis) destroyed the organic ligands the diffraction patterns started to fluctuate. We assumed that fluctuating structures do not represent the pristine structure.

Electron-beam damage in protected metallic clusters is the main physical limit for their analysis at atomic resolution. The initial damage arises in the ligands produced by an inelastic scattering of electrons resulting in a radiolysis damage mechanism. Subsequently, once the ligands have been destroyed, the metallic clusters become metastable and a high density of delocalized electrons is generated producing knock-on displacement. In order to reduce the radiation damage we used for previous works low voltage (80 kV), low temperature, rapid acquisition in aberration-corrected high angle annular dark field (HAADF) STEM imaging, and low dose, and herein we present a low-dose rapid nanobeam electron diffraction.[12,13] In the past we have demonstrated effective determination of protected clusters $Au_{144}(SR)_{60}$ and $Au_{130}(SR)_{50}$ by using quasi-parallel electron diffraction in individual clusters registered in static HAADF−STEM images at low voltages (80 kV).[12,13] In those analyses the patterns were collected irradiating continuously the clusters and producing damage after a few seconds due to the radiolysis damage in the ligands. The new method proposed herein allows the collection of patterns in a rapid scanning of nanobeam diffraction patterns over areas in which the clusters are dispersed. The low dose reduces significantly the radiolysis damage before the generation of the subsequent knock-on damage. The decrease of voltage is one of the methods of reducing radiation when radiolysis mechanism is present, this reduction is inversely proportional to the square of the acceleration voltage $(1/E_0^2)$, which results in a reduction of energy dissipation for organic materials.[27,28] Typically, radiolysis is produced in organic materials by a bond breakage and escape of light atoms, particularly in this work for the MBA group: hydrogen, carbon and oxygen atoms. The complete destruction of the protected cluster would be observed in the deterioration of the electron diffraction patterns; however using a fast scanning diffraction radiolysis damage can be avoided. The dose measured can be defined as product of the beam current density and the exposure time (C/cm^2). Experimental parameters considered to produce radiation damage due to the increase of number of electrons incident on the specimen are diameter of the incident beam (d), the beam current (I), and the irradiation time (T). Then, the dose can be defined as $D = IT/d^2$.[29,30] Regarding the knock-on and radiolysis damage mechanism, the primary damage is radiolysis due to the pMBA elements and subsequently knock-on in the metallic atoms. In this way, for knock-on damage the voltage used in our experiments is above the minimum transfer energy required for modifying or removing pMBA elements. However, decreasing the electron dose the ligands are less susceptible to be damage and as a consequence keep the stability of the metallic clusters. Therefore, we consider the primary mechanism, radiolysis, as the critical factor rather than the reduction of energy, since we have observed damage as well for other clusters studied in previous works.[12,13] In summary, in the current work, we reduce the electron dose and increase the speed of acquisition to collect electron diffraction patterns before induce damage initially produced by radiolysis. In our experiments, the patterns are registered using a low electron dose ranging from 1.4 to 2.8 pA/cm^2 at 200 kV, all the patterns were recorded in a sequence of scanning and recording of 0.1 nm point-to-point and at 0.1 s of acquisition time, respectively. Finally, it is remarkable the detective quantum efficiency (DQE) of the CMOS camera used which can register a reduced dose of electrons per pixel and eliminating the saturation and

DOI: 10.1021/acs.jpcc.5b09524
J. Phys. Chem. C XXXX, XXX, XXX−XXX

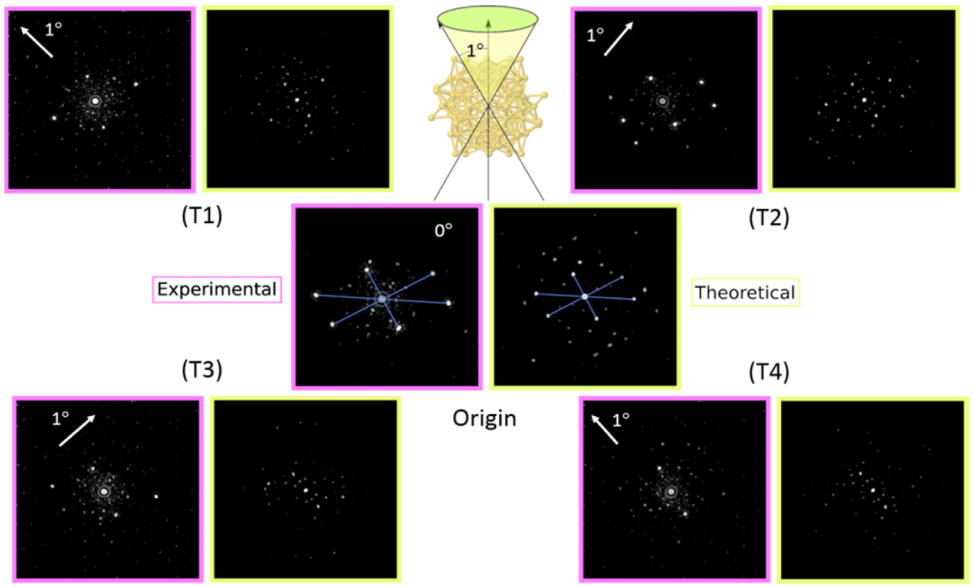

Figure 4. Set of experimental and simulated patterns extracted from a metallic clusters and its surroundings patterns. A good agreement for indexing the experimental patterns with simulations of zero (origin) and tilting one degree out of an axial axis (T1−T4).

blooming/streaking artifacts typically observed in conventional CCD cameras in electron diffraction patterns.[31,32]

For the digital analysis of the patterns, we have used an orthogonal supercell size, whose dimensions were 36 × 36 × 18 Å, chosen carefully in order to avoid the effects of periodicity. The initial *z* orientation considered in the nanobeam diffraction simulations was the 5-fold symmetry structure. By guiding our algorithm on this structure, we have rotated the particle in five directions, *x*, *y*, *xy*, $^{1}/_{2}xy$, and $x^{1}/_{2}y$, in order to obtain a diffraction pattern in each grade. Totally, we obtained 180 rotations per direction. Both the simulated and the experimental diffraction patterns were deconvoluted using an iterative Richardson − Lucy algorithm[33,34] implemented in the *G′*MIC program.[35] By a careful examination of our experimentally acquired nanobeam diffraction patterns using ultralow dose acquisition, in Figure 3a−c we can clearly observe that they exhibit striking similarities with the corresponding simulated diffraction patterns in Figure 3d−f, quantifiable based on the good match related to the angles between the *g*-vectors. It is pertinent to remark that our method is based on quantitative comparison between spot positions and angles between the experimental and the simulated diffraction patterns based on the considered structural model. These symmetries in the simulated and the experimental diffraction patterns are key points for the extraction of structural data from the Au_{102} nanocluster core. The "diffracting unit" of the cluster is the D_{5h}-symmetric core consisting of 79 Au atoms. The core is protected by a gold−thiolate layer of composition $Au_{23}(p\text{-MBA})_{44}$ having the total structural formula $Au_{79}[Au_{23}(p\text{-MBA})_{44}]$.[1,15] This is quantitatively emphasized in the distances measured between the transmitted spots and the observed reflections in Figure 3a−f, as well as the angles between the *g*-vectors, summarized in Table 1.

It is important to mention that additional errors in angle measurements may occur following the image processing algorithm. The variations introduced during noise removal and deblurring procedures are a minimization problem, which are always associated with a variation of dispersion of the data. These variations can generate some small oscillations in the positioning of the geometric center of spots in the image. However, for the nanoclusters labeled as A, B, and C, the match related to the angles between the *g*-vectors in the experimental and simulated patterns are very good. As we mentioned earlier, the brightest spots in the acquired experimental patterns originate from the atomic structure of the $Au_{102}(p\text{-MBA})_{44}$ nanocluster core. No additional spots have been observed in the experimental patterns corresponding to the Au atoms comprised in the staple RS−Au−SR motif (i.e., the outermost 23 Au atoms bound to the 44 groups (*p*-MBA) ligands on the cluster shell), since, as observed in our structural model, they are positioned relatively irregular with respect to each other. The observed additional spots in the experimental patterns may be explained on the basis of the following: (i) influence induced by the noise in the images; (ii) presence of amorphous C substrate supporting the Au nanoclusters; (iii) probe size, where the minimum probe diameter used in our experiment has been 3 nm (see Figure S4). Therefore, some extra reflections may be introduced by the probe converging on more than one particle at a time. It is important to mention that, unlike bulk crystals, small systems like $Au_{102}(p\text{-MBA})_{44}$ nanoclusters only show a limited amount of possible electron diffraction patterns sets. It has been well documented in the literature that morphological changes in the nanoclusters structure can be induced either by the interaction between the electron beam and the nanoparticle, via thermal effects, but also the interaction between the amorphous carbon film substrate and the nanoclusters.[36,37] However, these morphological changes in the nanoclusters structure would induce contrast changes in the nanoclusters diffraction patterns.[38,39] In any case, with careful consideration of the experimental parameters, like in the case of our acquired nanobeam diffraction method, we can obtain extremely reliable diffraction patterns that can be correlated to *ab initio* cluster models, without ambiguity. In contrast with regular crystals, due to the small volume of the clusters, it is visible that the experimental electron diffraction patterns contain few reflections.

The fast scanning method is synchronized with the CMOS acquisition under recording mode. Every point scanned across

DOI: 10.1021/acs.jpcc.5b09524
J. Phys. Chem. C XXXX, XXX, XXX−XXX

the area produces a single pattern such that the whole area will produce thousands of patterns. Every point during the scanning produces one diffraction pattern. We have observed that once the e-beam moves on metallic particle, the particle oscillates in a canonical shape. Figures S6 and S7 of the Supporting Information show a schematic illustration of the scanning method in the area and the diffraction patterns collected every 0.1 s. The map of patters in the area within the cluster and its surrounding shows a good agreement when is indexed with the simulations of the cluster disoriented 1 degree out of its axis. The Figure 4 shows a set of simulated and experimental NBD patterns extracted from a whole field of view, which have been taken from a region in which the simulated patterns show the metallic cluster disoriented 1 degree out of its axial axis as shown in the Figure S7. The video (video1) available in the Supporting Information shows the oscillation of 1 degree with a conical shape. Experimentally, we have observed transformation in the diffraction patterns *after more than 2 s of irradiation* and using the same dose or by increasing the beam current above 10 pA/cm^2. In this way, maximum energy transferred at different energies has been calculated (see Figure S8 of the Supporting Information) considered the knock-on mechanism.[30] The effect on the transformation is observed as a totally damage of the metallic clusters when they are irradiated for long exposure times. For scanning diffraction, the diffraction patterns disappear giving the diffraction of the amorphous carbon film. In scanning transmission electron microscopy (STEM) using the high annular angle dark field detector (HAADF) we have observed a separation of atoms as shown in Figure S9a. On the other hand, when we perform high resolution TEM and the ligands are removed some clusters are agglomerated to form a regular gold nanoparticle. In this way, we have performed off axis electron holography to measure the thickness of the metallic clusters and observed the coalescence as shown and explained in Figure S9c. It is well-known that in electron diffraction analysis, in contrast to X-ray crystallography, the intensity of an electron diffraction spot cannot be simply correlated to the square of the structure factor, due to the dynamical effects.[17] Our indexation method is related only to a direct comparison between the experimentally measured distances and the simulated ones. Our method for ultralow dose nanobeam diffraction patterns indexation proves to be a reliable method for the structural and crystallographic characterization of small nanoclusters sensitive to electron beam, being able to "map" from a crystallographic point of view tens and even hundreds of clusters in a single scan of the electron beam on a pre-established area.

4. CONCLUSIONS

We have shown an ultrafast nanobeam diffraction acquisition method for the $Au_{102}(p\text{-MBA})_{44}$ nanoclusters. Using this method, we have been able to demonstrate that structural information can be obtained for the $Au_{102}(p\text{-MBA})_{44}$ nanoclusters by comparing the experimental diffraction patterns with the simulated ones. The highlight of the paper is the low dose, fast acquisition of the experimental nanobeam diffraction collected on individual nanoclusters, in contrast with the classical acquisition of collective diffraction data used in X-ray analysis. We have been able to obtain a remarkable agreement between the experimental and simulated patterns, by a quantitative comparison of spot positions and angles between experimental and simulated patterns. We have demonstrated this methodology on a challenging problem, namely resolving the structure of the $Au_{102}(p\text{-MBA})_{44}$ nanoclusters. By demonstrating its application toward resolving this nanocluster structure, the method can be extended on a variety of small nanoclusters systems susceptible to electron beam damage.

■ ASSOCIATED CONTENT

Supporting Information

The Supporting Information is available free of charge on the ACS Publications website at DOI: 10.1021/acs.jpcc.5b09524.

ESI−MS experimental details, NBD patterns acquired with a typical CCD camera, details related to the image processing algorithm (PDF)

Video showing the whole area of the electron diffraction patterns (MPG)

■ AUTHOR INFORMATION

Corresponding Author

*(M.J.-Y.) E-mail: miguel.yacaman@utsa.edu.

Notes

The authors declare no competing financial interest.

■ ACKNOWLEDGMENTS

This project was supported by grants from the National Center for Research Resources (5 G12RR013646-12) and the National Institute on Minority Health and Health Disparities (G12MD007591) from the National Institutes of Health and the Welch Foundation (Grant No. AX-1615). U.S. acknowledges the scholarship of Conacyt No. 250836. The authors would like to acknowledge Dr. D. Black for obtaining the ESI−MS data. R.L.W. acknowledges support from a Welch Foundation Grant (AZ-1857).

■ REFERENCES

(1) Jadzinsky, P. D.; Calero, G.; Ackerson, C. J.; Bushnell, D. A.; Kornberg, R. D. Structure of a thiol monolayer-protected gold nanoparticle at 1.1 A resolution. *Science* **2007**, *318*, 430−433.

(2) Marjomaki, V.; Lahtinen, T.; Martikainen, M.; Koivisto, J.; Malola, S.; Salorinne, K.; Pettersson, M.; Häkkinen, H. Site-specific targeting of enterovirus capsid by functionalized monodisperse gold nanoclusters. *Proc. Natl. Acad. Sci. U. S. A.* **2014**, *111*, 1277−1281.

(3) Mustalahti, S.; Myllyperkio, P.; Malola, S.; Lahtinen, T.; Salorinne, K.; Koivisto, J.; Häkkinen, H.; Pettersson, M. Molecule-like photodynamics of Au102(pMBA)44 nanocluster. *ACS Nano* **2015**, *9*, 2328−2335.

(4) Bond, G. C. In *Gold nanoparticles in physics, chemistry and biology*; Louis, C., Pluchery, O., Eds.; Imperial College Press: London, 2012.

(5) Ladd, M.; Palmer, R. *Structure determination by x-ray crystallography*, 5th ed, Springer: New York, 2013.

(6) Zhu, M.; Aikens, C. M.; Hollander, F. J.; Schatz, G. C.; Jin, R. Correlating the crystal structure of a thiol-protected Au25 cluster and optical properties. *J. Am. Chem. Soc.* **2008**, *130*, 5883−5885.

(7) Heaven, M. W.; Dass, A.; White, P. S.; Holt, K. M.; Murray, R. W. Crystal structure of the gold nanoparticle [N(C8H17)4][Au25(SCH2CH2Ph)18]. *J. Am. Chem. Soc.* **2008**, *130*, 3754−3755.

(8) Qian, H. F.; Eckenhoff, W. T.; Zhu, Y.; Pintauer, T.; Jin, R. C. Total structure determination of thiolate-protected Au38 nanoparticles. *J. Am. Chem. Soc.* **2010**, *132*, 8280−8281.

(9) Wang, Z. W.; Toikkanen, O.; Quinn, B. M.; Palmer, R. E. Real-space observation of prolate monolayer-protected au38 clusters using aberration-corrected scanning transmission electron microscopy. *Small* **2011**, *7*, 1542−1545.

(10) Egerton, R. F.; Li, P.; Malac, M. Radiation damage in the TEM and SEM. *Micron* **2004**, *35*, 399−409.

(11) Azubel, M.; Koivisto, J.; Malola, S.; Bushnell, D.; Hura, G. L.; Koh, A. L.; Tsunoyama, H.; Tsukuda, T.; Pettersson, M.; Hakkinen,

DOI: 10.1021/acs.jpcc.5b09524
J. Phys. Chem. C XXXX, XXX, XXX−XXX

H.; et al. Nanoparticle imaging. Electron microscopy of gold nanoparticles at atomic resolution. *Science* **2014**, *345*, 909−912.
(12) Bahena, D.; Bhattarai, N.; Santiago, U.; Tlahuice, A.; Ponce, A.; Bach, S. A.; Yoon, B.; Whetten, R. L.; Landman, U.; Jose-Yacaman, M. STEM electron diffraction and high resolution images used in the determination of the crystal structure of $Au_{144}(SR)_{60}$ cluster. *J. Phys. Chem. Lett.* **2013**, *4*, 975−981.
(13) Tlahuice-Flores, A.; Santiago, U.; Bahena, D.; Vinogradova, E.; Conroy, C. V.; Ahuja, T.; Bach, S. B. H.; Ponce, A.; Wang, G.; Jose-Yacaman, M.; et al. Structure of the thiolated Au130 cluster. *J. Phys. Chem. A* **2013**, *117*, 10470−10476.
(14) Li, Y.; Galli, G.; Gygi, F. Electronic structure of thiolate-covered gold nanoparticles: Au102(MBA)44. *ACS Nano* **2008**, *2*, 1896−1902.
(15) Walter, M.; Akola, J.; Lopez-Acevedo, O.; Jadzinsky, P. D.; Calero, G.; Ackerson, C. J.; Whetten, R. L.; Gronbeck, H.; Häkkinen, H. A unified view of ligand-protected gold clusters as superatom complexes. *Proc. Natl. Acad. Sci. U. S. A.* **2008**, *105*, 9157−9162.
(16) Rauch, E. F.; Véron, M.; Portillo, J.; Bultreys, D.; Maniette, Y.; Nicolopoulos, S. Automatic crystal orientation and phase mapping in TEM by precession diffraction. *Microsc. Anal.* **2009**, *22*, S5−S8.
(17) Midgley, P.; Eggeman, A. S. Precession electron diffraction - a topical review. *IUCrJ* **2015**, *2*, 126−136.
(18) Nanomegas Company Home Page. http://www.nanomegas.com/ (accessed: 12, 2015).
(19) The company Tietz Video and Image Processing Systems company, TemCam-F416 camera documentation. http://www.tvips.com/pdfs/TemCam-F416.pdf (accessed: 12, 2015).
(20) Nannenga, B. L.; Shi, D.; Leslie, A. G.; Gonen, T. High-resolution structure determination by continuous-rotation data collection in MicroED. *Nat. Methods* **2014**, *11*, 927−930.
(21) Stadelmann, P. A. EMS - A software package for electron diffraction analysis and HREM image simulation in materials science. *Ultramicroscopy* **1987**, *21*, 131−145.
(22) Jems home page. http://cime.epfl.ch/research/jems (accessed: 12, 2015).
(23) Krakow, W.; Jose-Yacaman, M.; Aragon, J. L. Observation of quasi-melting at the atomic-level in Au nanoclusters. *Phys. Rev. B: Condens. Matter Mater. Phys.* **1994**, *49*, 10591−10596.
(24) Marks, L.; Smith, D. Direct surface imaging in small metal particles. *Nature* **1983**, *303*, 316−317.
(25) Iijima, S.; Ichihashi. Structural instability of ultrafine particles of metals. T. *Phys. Rev. Lett.* **1986**, *56*, 616−619.
(26) Ajayan, S.; Marks, L. Quasimelting and phases of small particles. *Phys. Rev. Lett.* **1988**, *60*, 585−587.
(27) Reimer, L.; Kohl, H. *Transmission electron microscopy: physics of image formation*; Springer Series in Optical Sciences; Springer: Berlin, 2008; pp 477−480.
(28) Egerton, R. F.; Li, P.; Malac, M. Radiation damage in the TEM and SEM. *Micron* **2004**, *35*, 399−409.
(29) Egerton, R. F. Control of radiation damage in the TEM. *Ultramicroscopy* **2013**, *127*, 100−108.
(30) Egerton, R. F.; McLeod, R.; Wang, F.; Malac, M. Basic questions related to electron-induced sputtering in the TEM. *Ultramicroscopy* **2010**, *110*, 991−997.
(31) Lee, Z.; Rose, H.; Lehtinen, O.; Biskupek, J.; Kaiser, U. Electron dose dependence of signal-to-noise ratio, atom contrast and resolution in transmission electron microscope images. *Ultramicroscopy* **2014**, *145*, 3−12.
(32) Stumpf, M.; Bobolas, K.; Daberkow, I.; Fanderl, U.; Heike, T.; Huber, T.; Kofler, C.; Maniette, Y.; Tietz, H. R. Design and characterization of 16 MegaPixel fiber optic coupled CMOS detector for transmission electron microscopy. *Microsc. Microanal.* **2010**, *16*, 856−857.
(33) Richardson, W. H. Bayesian-based iterative method of image restoration. *J. Opt. Soc. Am.* **1972**, *62*, 55−59.
(34) Lucy, L. B. An iterative technique for the rectification of observed distributions. *Astron. J.* **1974**, *79*, 745−754.
(35) Tschumperlé, D. *GREYC's magic image converter version 1.5.1.6, 2012*; University of Nice-Sophia: Antipolis, France, 2002.
(36) Wang, Z. W.; Palmer, R. E. Experimental evidence for fluctuating, chiral-type Au55 clusters by direct atomic imaging. *Nano Lett.* **2012**, *12*, 5510−5514.
(37) Williams, P. Motion of small gold clusters in the electron microscope. *Appl. Phys. Lett.* **1987**, *50*, 1760−1762.
(38) Ben-David, T.; Lereah, Y.; Deutscher, G.; Penisson, J.; Bourret, A.; Kofman, R.; Cheyssac, P. Correlated orientations in nanocrystal fluctuations. *Phys. Rev. Lett.* **1997**, *78*, 2585−2587.
(39) Tvedte, L. M.; Ackerson, C. J. Size-focusing synthesis of gold nanoclusters with p-mercaptobenzoic acid. *J. Phys. Chem. A* **2014**, *118*, 8124−8128.

DOI: 10.1021/acs.jpcc.5b09524
J. Phys. Chem. C XXXX, XXX, XXX−XXX